Thermodynamic properties of $SmMnO_3$, $Sm_{0.55}Sr_{0.45}MnO_3$ and $Ca_{0.85}Sm_{0.15}MnO_3$

2008 J. Phys.: Condens. Matter 20 415201

(http://iopscience.iop.org/0953-8984/20/41/415201)

J. Phys.: Condens. Matter **20** (2008) 415201 (6pp) doi:10.1088/0953-8984/20/41/415201

Thermodynamic properties of $SmMnO_3$, $Sm_{0.55}Sr_{0.45}MnO_3$ and $Ca_{0.85}Sm_{0.15}MnO_3$

Renu Choithrani[1], N K Gaur[1] and R K Singh[2]

[1] Department of Physics, Barkatullah University, Bhopal (MP) 462026, India
[2] School of Basic Sciences, MATS University, Raipur (CG) 492002, India

E-mail: renuchoithrani@gmail.com

Received 17 June 2008
Published 5 September 2008
Online at stacks.iop.org/JPhysCM/20/415201

Abstract

We have investigated thermodynamic properties of the perovskite Sm(Ca, Sr)MnO_3 manganites, probably for the first time, using the rigid ion model (RIM) after modifying its framework to incorporate the van der Waals attraction and the short-range Hafemeister–Flygare type overlap repulsion operating between the first and second neighbour ions. We have found that the evaluated thermodynamic properties reproduce the corresponding experimental data well, implying that the modified RIM properly represents the elastic nature of these perovskite manganite systems. The results of the present investigation can be further improved by including the ferromagnetic spin wave contribution and Jahn–Teller distortion effect in the framework of the modified RIM.

1. Introduction

During the past few decades, the effects of strongly correlated electrons and/or charge ordered (CO) phenomena have appeared in some major developments beginning with the mechanism of high T_c superconductivity [1] in cuprates followed (a decade later) by the observation of colossal magnetoresistance (CMR) [2] in perovskite manganites [3–5]. These manganites exhibit a rich phase diagram including different types of ordering phenomena and ground states, such as charge order, orbital order, and antiferromagnetic (AFM) or ferromagnetic (FM) insulators or metals [6, 7]. The CMR phenomena has mostly been found and studied in the perovskite manganites with the general formula $RE_{1-x}AE_xMnO_3$ (where RE = La, Pr, Nd, Sm, Eu, Gd, Ho, Tb, Y etc and AE = Sr, Ca, Ba, Pb). In the present investigation, we have focused our attention on the pure $SmMnO_3$ and the electron-doped $Sm_{1-x}Sr_xMnO_3$ ($x = 0.45$) and $Ca_{1-x}Sm_xMnO_3$ ($x = 0.15$) manganites. These manganites exhibit several interesting and anomalous features due to the competition among the electronic phases, ferromagnetic metallic (FM) state and charge-orbital-ordered (CO/OO) states with the collectively Jahn–Teller coupled lattice deformations (as reviewed in detail by Tokura [4]).

The crystal structure of $SmMnO_3$ (space group *pnma*) has an orthorhombic perovskite structure [8] with four formula units per unit cell and four 3d electrons: three t_{2g} and one e_g electrons [7]. Since three t_{2g} electrons form an orbitally closed shell, many physical properties are believed to be governed by its e_g electrons. The occurrence of the spin and orbital ordered state has been understood in terms of the cooperative Jahn–Teller (JT) distortion [9]. The pure $SmMnO_3$ exhibits a Jahn–Teller distorted orthorhombic structure and shows a sharp peak in the specific heat at ∼59 K due to the A-type AF ordering [10] and this feature is remarkable in the experimental specific heat.

The phase diagram of $Sm_{0.55}Sr_{0.45}MnO_3$ shows two critical end points in zero magnetic field (128.6 and 113.3 K) [11]. The crystal structure of $Sm_{0.55}Sr_{0.15}MnO_3$ is orthorhombic perovskite as determined from XRD data by Abdulvagidor *et al* [11]. The $Ca_{0.85}Sm_{0.15}MnO_3$ manganite has been found to exhibit some unique properties, such as the structural transformation from an orthorhombic Pnma phase to a monoclinic $P2_1/m$ phase [12] on lowering the temperature to 115 K [13]. Also, the low-temperature phase of $Ca_{0.85}Sm_{0.15}MnO_3$ is a C-type antiferromagnet, which possesses, however, a weak ferromagnetic moment [13]. The temperature dependence of the specific heat of $Ca_{0.85}Sm_{0.15}MnO_3$ reveals one well-pronounced anomaly at $T \sim 115$ K [12–14].

The study of pure $SmMnO_3$ and doped Sm(Ca, Sr)MnO_3 perovskite manganites is motivated by their interesting features of the CMR effect, antiferromagnetic (low temperature) ground state and strong Jahn Teller distortion. There is much experimental evidence indicating the importance of the

electron–lattice coupling in manganese oxides [15–17] from which one can see that there is a close relation between the lattice dynamics and the electronic and magnetic properties. These features indicate the necessity of understanding the interaction mechanism and physical properties of these manganites.

Recently, we have successfully shown the thermodynamic behaviour of some manganites [18–20], by using a modified rigid ion model (MRIM) [18–20]. The major contribution to the pair potential of MRIM is contributed by the long-range (LR) Coulomb attraction, which is counterbalanced by the short-range (SR) overlap repulsion having their origin in the Pauli exclusion principle. This SR interaction is expressed by a Hafemeister–Flygare (HF) [21] type overlap repulsion effective up to the second neighbour ions. This potential also incorporates the effects of the van der Waals (vdW) attraction (Tosi and Fumi [22]) arising from the dipole–dipole (d–d) and dipole–quadrupole (d–q) interactions, whose coefficients are estimated from the Slater–Kirkwood variational (SKV) [23] approach, which treats both the ions (cations and anions) as polarizable. Motivated from such a realistic and qualitative representation of the interionic potential and its versatile applicability to describing the cohesive and physical properties of solids and alloys (Singh [24] and Varshney *et al* [25]), we thought it pertinent to apply this MRIM, probably for the first time, to explore the thermodynamic properties of $SmMnO_3$, $Sm_{0.55}Sr_{0.45}MnO_3$ and $Ca_{0.85}Sm_{0.15}MnO_3$, as very scant attention has been paid on them by theoretical investigators. The interaction potential of the MRIM is described in section 2. The computed results are presented and discussed in section 3.

2. Essential formalism of MRIM

We have formulated the modified rigid ion model (MRIM) [18–20] by incorporating the effects of the long-range (LR) Coulomb attraction, the short-range (SR) Hafemeister–Flygare (HF) [21] type overlap repulsion effective up to the second neighbour ions and the van der Waals (vdW) attraction due to the dipole–dipole (d–d) and dipole–quadrupole (d–q) interactions in the framework of the RIM [24, 26]. The total cohesive energy (ϕ) of the MRIM is expressed as [18–20]:

$$\phi = -\frac{e^2}{2}\sum_{kk'} Z_k Z_{k'} r_{kk'}^{-1} + \Bigg[nb_1\beta_{kk'}\exp\{(r_k + r_{k'} - r_{kk'})/\rho_1\} + \frac{n'}{2}b_2[\beta_{kk}\exp\{(2r_k - r_{kk})/\rho_2\} + \beta_{k'k'}\exp\{(2r_{k'} - r_{k'k'})/\rho_2\}]\Bigg] - \sum_{kk'} c_{kk'} r_{kk'}^{-6} - \sum_{kk'} d_{kk'} r_{kk'}^{-8}. \quad (1)$$

Here, $k(k')$ denote the type of $k(k')$ ions. In the orthorhombic perovskite structure, k represents cations (A, B) and k' denotes the type of (O_1, O_2) ions with general formula ABO_3 (such as $SmMnO_3$). The summation in the first, fourth and fifth terms in equation (1) is performed over all the kk' ions. The second and third terms represent the short-range HF type overlap repulsion expressed as an exponential function of the separations $(r_k + r_{k'} - r_{kk'})$, $(2r_k - r_{kk})$ and $(2r_{k'} - r_{k'k'})$. The symbols $Z_K(Z_{k'})$ and $r_k(r_{k'})$ are the ionic charges and radii of the $k(k')$ ions. $n(n')$ represent the number of the first (second) neighbour ions. $\beta_{kk'}$ are the Pauling coefficients [27]:

$$\beta_{kk'} = 1 + (z_k/n_k) + (z_{k'}/n_{k'}) \quad (2)$$

with $z_k(z_{k'})$ and $n_k(n_{k'})$ as the valence and number of electrons in the outermost orbit of $k(k')$ ions. In equation (1), $r_{kk'}$ and $r_{kk}(=r_{k'k'})$ are, respectively, the first and second neighbour separations and their values are obtained for Sm substitutions (x) using the well known Vegard's law [28].

In equation (1), the first term represents the long-range Coulomb attraction, the second and third terms are the short-range HF [21] type overlap repulsion and the fourth and fifth terms are the vdW attraction energies due to d–d and d–q interactions, whose significance has been shown from the qualitative and quantitative analysis for some other systems of solids by Tosi and others [22]. The symbols $c_{kk'}$ and $d_{kk'}$ are the corresponding vdW coefficients, whose values are determined by using their expressions [18–20] derived from the Slater–Kirkwood variational (SKV) [23] method and by treating both the cations and anions as polarizable:

$$c_{kk'} = (3e\hbar\alpha_k\alpha_{k'}/2m)[(\alpha_k/N_k)^{1/2} + (\alpha_{k'}/N_{k'})^{1/2}]^{-1} \quad (3)$$

$$d_{kk'} = (27e\hbar^2\alpha_k\alpha_{k'}/8m)[(\alpha_k/N_k)^{1/2} + (\alpha_{k'}/N_{k'})^{1/2}]^2 \times [(\alpha_k/N_k)^{1/2} + \tfrac{20}{3}(\alpha_k\alpha_{k'}/N_kN_{k'})(\alpha_{k'}/N_{k'})]^{-1} \quad (4)$$

where m and e are the mass and charge of electron, respectively. $\alpha_k(\alpha_{k'})$ are the electronic polarizabilities of $k(k')$ ions; $N_k(N_{k'})$ are the effective number of electrons responsible for the polarization of $k(k')$ ions. The values of $c_{kk'}$ and $d_{kk'}$ are evaluated using the equations (3) and (4) and following the procedure adopted in our recent papers [19, 20].

The model parameters (hardness (b) and range (ρ)) are determined from the equilibrium condition:

$$[\mathrm{d}\phi(r)/\mathrm{d}r]_{r=r_0} = 0 \quad (5)$$

and the bulk modulus:

$$B = (9Kr_0)^{-1}[\mathrm{d}^2\phi(r)/\mathrm{d}r^2]_{r=r_0}. \quad (6)$$

Here, r_0 and r are the interionic separations in the equilibrium and otherwise states of the system, respectively. The symbol K is the crystal structure constant.

The values of the input data (r_0, B) for the evaluation of the four disposable model parameters (b_1, ρ_1) and (b_2, ρ_2) corresponding to the ionic bonds Mn–O and Sm/Sr or Ca–O for different compositions (x = 0.45 and 0.15) and temperatures 15 K $\leqslant T \leqslant$ 300 K [19] have been obtained from the well known Vegard's law using their experiment data from [10–12, 29–32]. The vdW coefficients $c_{kk'}$ and $d_{kk'}$ are evaluated from the SKV [23] method for the present manganites. The values of these model parameters (b_1, p_1) and (b_2, p_2) are depicted in tables 1–3 for $SmMnO_3$, $Sm_{0.55}Sr_{0.45}MnO_3$ and $Ca_{0.85}Sm_{0.15}MnO_3$ perovskites, respectively, and used to describe various physical properties of the present system of pure and doped manganites.

Table 1. Model parameters and thermodynamic properties of $SmMnO_3$.

	Model parameters				Thermodynamic properties					
T (K)	Mn–O ρ_1 (Å)	Mn–O b_1 (10^{-12} erg)	Sm–O ρ_2 (Å)	Sm–O b_2 (10^{-12} erg)	ϕ (eV)	f (10^4 dyn cm^{-1})	β (10^{-12} dyn^{-1} cm^2)	υ_0 (THz)	θ_D (K)	γ
15	0.616	1.868	0.804	2.121	−143.631	11.98	3.067	9.125	437.97	2.09
60	0.615	1.862	0.803	2.117	−143.671	12.03	3.057	9.141	438.74	2.09
105	0.614	1.856	0.801	2.114	−143.712	12.07	3.048	9.157	439.51	2.10
195	0.612	1.845	0.799	2.106	−143.792	12.15	3.029	9.189	441.04	2.12
240	0.611	1.839	0.798	2.103	−143.832	12.20	3.019	9.205	441.80	2.13
300	0.610	1.831	0.796	2.098	−143.885	12.25	3.007	9.226	442.82	2.14
(Expt)	—	—	—	—	(−140.52)[a]	—	—	(8.58)[b]	(465)[c]	(2–3)[d]

[a] Reference [33]; [b] reference [34]; [c] reference [10]; [d] reference [35].

Table 2. Model parameters and thermodynamic properties of $Sm_{0.55}Sr_{0.45}MnO_3$.

	Model parameters				Thermodynamic properties					
T (K)	Mn–O ρ_1 (Å)	Mn–O b_1 (10^{-12} erg)	Sm/Sr–O ρ_2 (Å)	Sm/Sr–O b_2 (10^{-12} erg)	ϕ (eV)	f (10^4 dyn cm^{-1})	β (10^{-12} dyn^{-1} cm^2)	υ_0 (THz)	θ_D (K)	γ
15	0.623	1.858	0.751	2.029	−144.920	12.91	3.029	9.469	454.47	2.32
60	0.622	1.852	0.750	2.026	−144.963	12.95	3.021	9.485	455.22	2.33
105	0.621	1.846	0.749	2.022	−145.005	12.99	3.013	9.500	455.96	2.34
195	0.619	1.834	0.746	2.015	−145.090	13.07	2.997	9.531	457.44	2.36
240	0.618	1.828	0.745	2.011	−145.133	13.12	2.989	9.547	458.18	2.37
300	0.617	1.821	0.744	2.006	−145.181	13.17	2.978	9.567	459.17	2.38
(Expt)					(−140.52)[a]			(8.58)[b]		(2–3)[c]

[a] Reference [33]; [b] reference [34]; [c] reference [35].

Table 3. Model parameters and thermodynamic properties of $Ca_{0.85}Sm_{0.15}MnO_3$.

	Model parameters				Thermodynamic properties					
T (K)	Mn–O ρ_1 (Å)	Mn–O b_1 (10^{-12} erg)	Ca/Sm–O ρ_2 (Å)	Ca/Sm–O b_2 (10^{-12} erg)	ϕ (eV)	f (10^4 dyn cm^{-1})	β (10^{-12} dyn^{-1} cm^2)	υ_0 (THz)	θ_D (K)	γ
15	0.495	1.128	0.577	1.557	−147.536	14.12	3.012	9.903	475.29	2.78
60	0.494	1.123	0.576	1.554	−147.555	14.16	3.005	9.918	476.00	2.79
105	0.493	1.119	0.575	1.551	−147.573	14.20	2.998	9.933	476.71	2.80
195	0.492	1.114	0.573	1.545	−147.610	14.28	2.984	9.962	478.12	2.82
240	0.491	1.105	0.572	1.542	−147.628	14.33	2.977	9.977	478.82	2.83
300	0.489	1.090	0.571	1.538	−147.652	14.38	2.967	9.996	479.76	2.85
(Expt)					(−140.52)[a]			(8.58)[b]		(2–3)[c]

[a] Reference [33]; [b] reference [34]; [c] reference [35].

The specific heat at constant volume (C_v) for $SmMnO_3$, $Sm_{0.55}Sr_{0.45}MnO_3$ and $Ca_{0.85}Sm_{0.15}MnO_3$ have been calculated at different temperatures (T) using the well known expression [18–20]:

$$C_v = 9R\left(\frac{T}{\theta_D}\right)^3 \int_0^{\frac{\theta_D}{T}} \frac{e^x x^4}{e^x - 1} dx. \quad (7)$$

The specific heat at constant pressure is calculated using [18]:

$$C_p = TV\alpha^2 B_T + C_v, \quad (8)$$

where α is the linear thermal expansion coefficient, B_T is the isothermal bulk modulus, and V is the unit cell volume.

In addition, we have computed the thermodynamic parameters, such as the cohesive energy (ϕ), molecular force constant (f), compressibility (β), Restrahalen frequency (υ_0), Debye temperature (θ_D) and Grüneisen parameter (γ) of $SmMnO_3$, $Sm_{0.55}Sr_{0.45}MnO_3$ and $Ca_{0.85}Sm_{0.15}MnO_3$ using their expressions reported elsewhere [18, 19]. The computed results thus obtained are presented and discussed below.

3. Computed results and discussion

Using the disposable model parameters listed in tables 1–3, the values of ϕ, f, β, υ_0, θ_D and γ are computed and depicted in tables 1, 2 and 3 for $SmMnO_3$, $Sm_{0.55}Sr_{0.45}MnO_3$ and $Ca_{0.85}Sm_{0.15}MnO_3$, respectively. The chief aim of the application of the present model is to reproduce the observed physical properties such as the transport and thermodynamic properties of perovskite manganites. Keeping this objective in view, we find that our results obtained for most of the transport properties are closer to the experimental data [10, 33–35] available only at 300 K. The cohesive energy is the measure of strength of the force binding the atoms together in solids. This

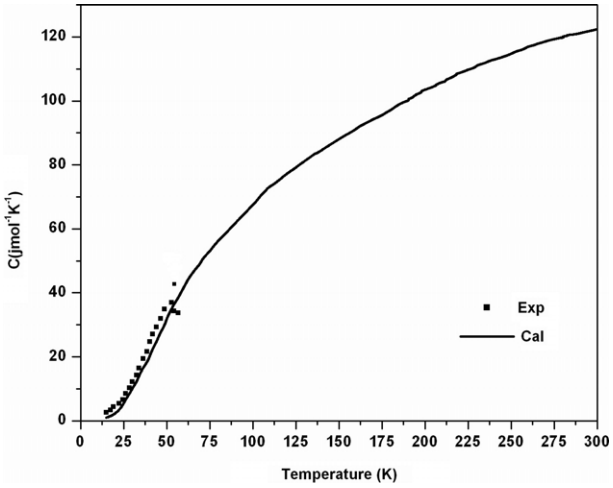

Figure 1. Variation of specific heat with temperature of $SmMnO_3$ where the solid line (——) and squares (■) represent the model calculation and experimental [10] values respectively.

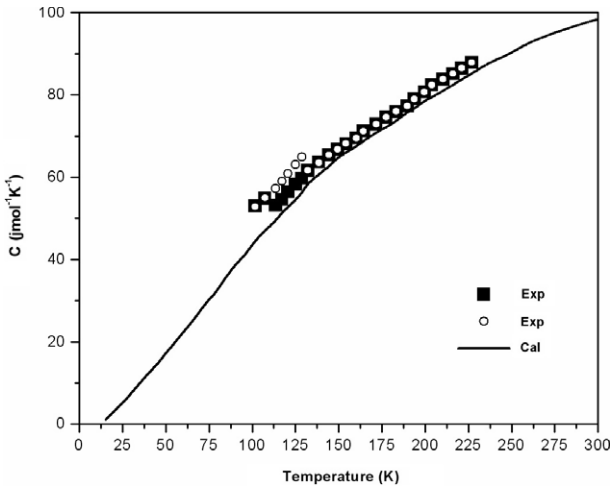

Figure 2. Variation of specific heat with temperature of $Sm_{0.55}Sr_{0.45}MnO_3$ where the solid line (——) and squares (■) and open circles (○) represent the model calculation and experimental [11] values respectively.

fact is exhibited from our cohesive energy results which follow the similar trend of variation with T, as is revealed by the bulk modulus that represents the resistance to volume change [32]. This feature is indicated from tables 1–3, which show that the values of the cohesive energy (ϕ) decreases from −143.885 eV for $SmMnO_3$ to −145.181 eV for $Sm_{0.55}Sr_{0.45}MnO_3$ and −147.652 eV for $Ca_{0.85}Sm_{0.15}MnO_3$ with Sr (Ca) dopings; the same trend of variation is also exhibited by the bulk modulus. Due to a lack of experimental data, we have compared the values of cohesive energy of pure $SmMnO_3$ with that of $LaMnO_3$ [33], which is a member of the same family. The negative values of cohesive energy show that the stability of these manganites is intact. It is also noticed from tables 1–3 that the values of hardness (b_1, b_2) and the stability (ϕ) decrease with temperature.

We have also calculated the values of the molecular force constants (f) and Restrahalen frequencies (υ_0) (see tables 1–3) and found that υ_0 increases with temperature (T). Since the Restrahalen frequency is directly proportional to the molecular force constant (f) therefore both of them vary with the temperature accordingly for different concentrations (x). The values of Restrahalen frequency are almost in the same range as that reported for the parent member $LaMnO_3$ ($\upsilon_0 = 8.58$ THz) [34]. The calculated value of Debye temperature (θ_D) for $SmMnO_3$ (442.822 K) is approximately in agreement with the experimental data (465 K) available only at room temperature [10]. The calculated values of (θ_D) for $SmMnO_3$, $Sm_{0.55}Sr_{0.45}MnO_3$ and $Ca_{0.85}Sm_{0.15}MnO_3$ at 300 K are 442.822, 459.170 and 479.764 K, which lie within the Debye temperature range (300–550 K) often found in perovskite manganites. The Grüneisen parameters (γ) obtained by us are found to lie between 2 and 3, which are similar to the values observed by Dai *et al* [35].

The specific heat (C) values calculated by us for pure $SmMnO_3$ at temperatures 15 K $\leqslant T \leqslant$ 300 K are displayed in figure 1 and found to be in good agreement with the measured data [10] at lower temperatures 15 K $\leqslant T \leqslant$ 60 K. Our results have followed a trend more or less similar to those exhibited by

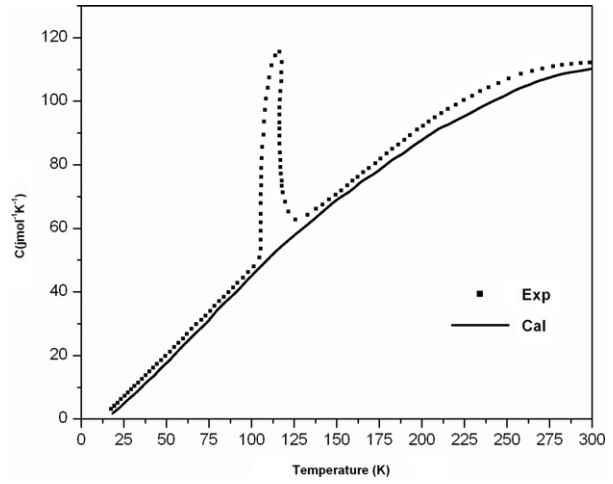

Figure 3. Variation of specific heat with temperature of $Ca_{0.85}Sm_{0.15}MnO_3$ where the solid line (——) and squares (■) represent the model calculation and experimental [12] values respectively.

the experimental curve at lower temperatures. A sharp peak is observed in the experimental specific heat curve at ∼59 K due to the A-type AF ordering. This feature is not revealed from our calculated results and this might be due to the exclusion of the spin correlation wave contribution in the MRIM. The change in Mn–O distance by the substitution of a Sm site by Sr or Ca increases θ_D and hence there is a consistent decrease in the specific heat values corresponding to the doping in both of the cases (see figures 2 and 3). Hence, the concentration (x) dependence of θ_D in $SmMnO_3$, $Sm_{0.55}Sr_{0.45}MnO_3$ and $Ca_{0.85}Sm_{0.15}MnO_3$ suggests that increased hole doping drives the system effectively towards the strong electron–phonon coupling regime. The present MRIM calculations yield similar specific heat values at low temperatures (below 60 K) where the acoustic phonons play an important role.

On doping Sr ($x = 0.45$) in $SmMnO_3$, the specific heat increases monotonically with temperature as shown in figure 2. The experimental specific heat results [11] for $Sm_{0.55}Sr_{0.45}MnO_3$ show two critical end points at 128.6 and 113.3 K which might be due to the ferromagnetic to paramagnetic transition. It is also seen from figure 2 that our theoretical results are in closer agreement with the available experimental [11] data in the middle range of temperature $100\ \text{K} \leqslant T \leqslant 225\ \text{K}$.

In the case of $Ca_{0.85}Sm_{0.15}MnO_3$, there are some special features which deserve detailed discussion. The specific heat also increases with temperature in $Ca_{0.85}Sm_{0.15}MnO_3$ as seen from figure 3. The MRIM results have fairly well reproduced the experimental specific heat data in the temperature ranges $15\ \text{K} \leqslant T \leqslant 100\ \text{K}$ and $120\ \text{K} \leqslant T \leqslant 300\ \text{K}$ except for the range $112\ \text{K} \leqslant T \leqslant 120\ \text{K}$, in which a cusp like anomaly occurs at 115 K in the specific heat curve (see figure 3); this feature corresponds to the phase transition from an orthorhombic *Pnma* to a monoclinic $P2_1/m$ as revealed from the neutron diffraction data [12]. However, the description of this anomaly is beyond the scope of our present model due to the inherent deficiency from not including the ferromagnetic spin wave contribution and Jahn–Teller distortion effect in our calculation.

4. Conclusion

The varied exposition of the temperature-dependent thermodynamical properties of perovskite manganites ($SmMnO_3$, $Sm_{0.55}Sr_{0.45}MnO_3$ and $Ca_{0.85}Sm_{0.15}MnO_3$) attained by us is remarkable in view of the inherent simplicity of the modified rigid ion model.

All this indicates the power and usefulness of the MRIM as having the potential to explain a variety of physical properties (such as cohesive, thermal, elastic, thermodynamic) of the pure and doped CMR materials. However, the efforts that have been devoted by many experimental workers to observe magnetic transitions and properties, to the best of our knowledge, only a few groups are involved with the study of temperature- and composition-dependent properties of perovskite manganites (or CMR) materials. On the basis of the overall descriptions, it may be concluded that our modified rigid ion model has reproduced thermodynamic properties that correspond well to the experimental data. The present results can be further improved by incorporating the effects of the ferromagnetic spin wave contribution and Jahn–Teller distortion in the framework of the MRIM in a future research programme.

Acknowledgments

The authors (particularly Renu Choithrani) are grateful to the Council of Scientific and Industrial Research (CSIR), New Delhi for the award of a Senior Research Fellowship (SRF) and the University Grants Commission (UGC), New Delhi for providing the financial support.

References

[1] Kumar N and Rao C N R 2003 *Phys. Rev.* B **4** 439
[2] Rao C N R, Arulraj A, Checthan A K and Ravean B 2000 *J. Phys.: Condens. Matter* **12** R83
[3] Tang F L and Zhang X 2006 *Phys. Rev.* B **73** 144401
Takashi H, Mohammad M, Adrian F, Adriana M, Seiji Y and Elbio D 2003 *Phys. Rev. Lett.* **90** 247203
Nikiforov A E, Popov S E and Shashkin S Y 2000 *Physica* B **276** 772
Katsufujj T and Takagi H 2001 *Phys. Rev.* B **64** 054415
[4] Tokura Y 2006 *Rep. Prog. Phys.* **69** 797
[5] Rodriguez E E, Proffen Th, Llobet A and Ryne J J 2005 *Phys. Rev.* B **71** 104430
[6] Torrance J B, Lacorre P, Nazzal A I, Ansaldo E J and Niedermayer Ch 1992 *Phys. Rev.* B **45** 8209
[7] Hemberger J, Brando M, When R, Ivanov V Yu, Mukhin A A, Balbashov A M and Loidl1 A 2004 *Phys. Rev.* B **69** 064418
[8] Kiichiro K, Tadashi N and Tetsuro N 1979 *Mater. Res. Bull.* **14** 1007
[9] Dabrowski B, Kolesnik S, Baszczuk A, Chmaissem O, Maxwell T and Mais J 2005 *J. Solid State Chem.* **178** 629
[10] Kimura T, Ishihara S, Shintani H, Arima T, Takahashi K T, Ishizaka K and Tokura Y 2003 *Phys. Rev.* B **68** 060403
[11] Abdulvagidov Sh B, Aliev A M, Gamzatov A G, Nizhankovskii V I, Modge H and Gorbenko O Yu 2006 *JETP Lett.* **84** 31–4
[12] Filippov D A, Levitin R Z, Vasil'ev A N and Voloshok T N 2002 *Phys. Rev.* B **65** 100404
[13] Martin C, Maignan A, Hervieu M, Raveau B, Jirák Z, Kurbakov A, Trounov V, André G and Bourée F 1999 *J. Magn. Magn. Mater.* **205** 184–98
[14] Vasil'ev A N, Voloshok T N and Suryanarayanan R 2001 *JETP Lett.* **73** 349
[15] Ibarra M R, Algarabel P A, Marquina C, Blasco J and Garcia J 1995 *Phys. Rev. Lett.* **75** 3541–4
[16] Kim K H, Gu J Y, Choi H S, Park G W and Noh T W 1996 *Phys. Rev. Lett.* **77** 1877
[17] Garland W 1970 *Physics of Acoustics* vol vii, ed W P Mason and R N Thurston (New York: Academic) p 52
[18] Choithrani R and Gaur N K 2008 *J. Magn. Magn. Mater.* **320** 612–6
Choithrani R and Gaur N K 2008 *J. Magn. Magn. Mater.* at press
[19] Gaur N K, Choithrani R and Srivastava A 2008 *Solid State Commun.* **145** 308–11
[20] Choithrani R, Gaur N K and Singh R K 2008 *Solid State Commun.* **147** 103–6
[21] Hafemiester D W and Flygare W H 1965 *J. Chem. Phys.* **43** 795
[22] Tosi M P and Fumi F G 1965 *J. Phys. Chem. Solids* **23** 359
Tosi M P 1964 *Solid State Phys.* **2** 1
[23] Slater J C and Kirkwood K G 1931 *Phys. Rev. Lett.* **37** 682
[24] Singh R K 1982 *Phys. Rep.* **85** 259
[25] Varshney D, Kaurav N, Kinge R and Singh R K 2007 *J. Phys.: Condens. Matter* **19** 236204
Varshney D, Kaurav N, Kinge R and Singh R K 2007 *J. Phys.: Condens. Matter* **19** 346212
[26] Kellerman E W 1940 *Phil. Trans. R. Soc.* A **238** 513
[27] Pauling L 1928 *Z. Kristallogr.* **67** 377
[28] Vegard L 1921 *Z. Phys.* **5** 17
[29] Mukhin A A, Travkin V D, Prokhorov A S, Balbashov A M, Hemberger J and Loidl A 2004 *J. Magn. Magn. Mater.* **96/97** 272–6
[30] Levin E M and Shand P M 2007 *J. Magn. Magn. Mater.* **311** 675–82

[31] Laverdier J, Jandl S, Mukhin A A, Ivanov V Yu, Ivanov V G and Iliev M N 2006 *Phys. Rev.* B **73** 214301
[32] Iliev M N, Abrashev M V, Laverdiere J, Jandl S, Gospodinov M M, Wang Y-Q and Sun Y-Y 2006 *Phys. Rev.* B **73** 064302
[33] Roger A De Souza, Saiful Islam M and Ivers-Tiffe E 1999 *J. Mater. Chem.* **9** 1621
Kovalova N N, Gavartin J L, Shluger A L and Stoneham A M 2002 *Physica* B **734** 312–3
[34] Fedorov I, Lorenzana J, Dore P, Marzi G De, Maselli P, Calvani P, Cheong S-W, Koval S and Migoni R 1999 *Phys. Rev.* B **60** 11875
[35] Dai P, Jiandi Z, Mook H A, Lion S H, Dowben P A and Plummer E W 1996 *Phys. Rev.* B **54** R3694